Journal of Human Evolution 118 (2018) 56–71

Contents lists available at ScienceDirect

Journal of Human Evolution

journal homepage: www.elsevier.com/locate/jhevol

The biting performance of *Homo sapiens* and *Homo heidelbergensis*

Ricardo Miguel Godinho [a, b, c, *], Laura C. Fitton [a, b], Viviana Toro-Ibacache [b, d, e], Chris B. Stringer [f], Rodrigo S. Lacruz [g], Timothy G. Bromage [g, h], Paul O'Higgins [a, b]

[a] Department of Archaeology, University of York, York, YO1 7EP, UK
[b] Hull York Medical School (HYMS), University of York, Heslington, York, North Yorkshire YO10 5DD, UK
[c] Interdisciplinary Center for Archaeology and Evolution of Human Behaviour (ICArHEB), University of Algarve, Faculdade das Ciências Humanas e Sociais, Universidade do Algarve, Campus Gambelas, 8005-139, Faro, Portugal
[d] Facultad de Odontología, Universidad de Chile, Santiago, Chile
[e] Department of Human Evolution, Max Planck Institute for Evolutionary Anthropology, Leipzig, Germany
[f] Department of Earth Sciences, Natural History Museum, London, UK
[g] Department of Basic Science and Craniofacial Biology, New York University College of Dentistry, New York, NY 10010, USA
[h] Departments of Biomaterials & Biomimetics, New York University College of Dentistry, New York, NY 10010, USA

ARTICLE INFO

Article history:
Received 15 March 2017
Accepted 19 February 2018
Available online 15 March 2018

Keywords:
Homo heidelbergensis
Homo sapiens
Paleoanthropology
Finite element analysis
Virtual anthropology

ABSTRACT

Modern humans have smaller faces relative to Middle and Late Pleistocene members of the genus *Homo*. While facial reduction and differences in shape have been shown to increase biting efficiency in *Homo sapiens* relative to these hominins, facial size reduction has also been said to decrease our ability to resist masticatory loads. This study compares crania of *Homo heidelbergensis* and *H. sapiens* with respect to mechanical advantages of masticatory muscles, force production efficiency, strains experienced by the cranium and modes of deformation during simulated biting. Analyses utilize X-ray computed tomography (CT) scan-based 3D models of a recent modern human and two *H. heidelbergensis*. While having muscles of similar cross-sectional area to *H. heidelbergensis*, our results confirm that the modern human masticatory system is more efficient at converting muscle forces into bite forces. Thus, it can produce higher bite forces than Broken Hill for equal muscle input forces. This difference is the result of alterations in relative in and out-lever arm lengths associated with well-known differences in midfacial prognathism. Apparently at odds with this increased efficiency is the finding that the modern human cranium deforms more, resulting in greater strain magnitudes than Broken Hill when biting at the equivalent tooth. Hence, the facial reduction that characterizes modern humans may not have evolved as a result of selection for force production efficiency. These findings provide further evidence for a degree of uncoupling between form and function in the masticatory system of modern humans. This may reflect the impact of food preparation technologies. These data also support previous suggestions that differences in bite force production efficiency can be considered a spandrel, primarily driven by the midfacial reduction in *H. sapiens* that occurred for other reasons. Midfacial reduction plausibly resulted in a number of other significant changes in morphology, such as the development of a chin, which has itself been the subject of debate as to whether or not it represents a mechanical adaptation or a spandrel.

1. Introduction

The Middle Pleistocene extinct species *Homo heidelbergensis* has been proposed as the ancestral species of *Homo sapiens* and *Homo neanderthalensis* (Stringer, 1983; Rightmire, 1998; Stringer, 2012; but see Bräuer, 2001; Stringer, 2016; Meyer et al., 2016). Crania included in the hypodigm of *H. heidelbergensis* have a long but low cranial vault with a mean cranial capacity of 1263 cm^3 (Schwartz and Tattersall, 2003; Lieberman, 2011). The face is very large (Rightmire, 1998; Freidline et al., 2012) and presents an extremely enlarged double-arched browridge that overhangs 'square' orbits that slope inferiorly and laterally at the inferior margins (Schwartz and Tattersall, 2003). The subnasal region is prognathic and significantly taller than that of *H. sapiens*. The maxillary root of the zygomatic arch is usually located above the first or second molar (Schwartz and Tattersall, 2003; Lieberman,

* Corresponding author.
E-mail address: ricardomiguelgodinho@gmail.com (R.M. Godinho).

https://doi.org/10.1016/j.jhevol.2018.02.010
0047-2484/

2011), unlike in Neanderthals (Trinkaus, 1987a), and in large individuals the infraorbital region lacks the concave canine fossa characteristic of *H. sapiens* (Freidline et al., 2012). Structurally, these anatomical features of fossils attributed to *H. heidelbergensis* are not markedly different from those found in Neanderthals (Lieberman, 2011). This has resulted in some specimens of *H. heidelbergensis* (e.g., Broken Hill, also known as Kabwe 1) having been considered as Neanderthal in the past (Tappen, 1978). It should be noted that material attributed to *H. heidelbergensis* s.l. includes fossils from Africa and Europe. As such, it has been argued that they may in fact represent different populations within a more complex, reticulated human evolutionary history than previously thought (Hublin et al., 2017). Thus, it has been proposed that African specimens may be included in a distinct species, *Homo rhodesiensis*, with European specimens being assigned to *H. heidelbergensis* (for a review, see Stringer, 2012).

The more gracile modern human cranium differs from those of *H. heidelbergensis* and *H. neanderthalensis* in several ways. When compared to *H. heidelbergensis* and Neanderthals, *H. sapiens* has an enlarged (relative to *H. heidelbergensis*, not Neanderthals), more globular cranial vault, with a mean cranial capacity of 1350 cm^3 (Lieberman, 2011), and a small gracile and orthognathic face, with reduced interorbital space, that is retracted under the anterior cranial fossa (Enlow and McNamara, 1973; Enlow and Hans, 1996; Lieberman et al., 2002; Trinkaus, 2003; Lieberman, 2011). This facial reduction in *H. sapiens* is associated with the presence of a canine fossa, a short oropharynx, more rectangular orbital cavities, and a chin (Enlow and McNamara, 1973; Enlow and Hans, 1996; Lieberman et al., 2002; Trinkaus, 2003; Lieberman, 2011). Additionally, recent *H. sapiens* is said to have generally reduced masticatory muscle cross-sectional areas relative to *H. neanderthalensis*, based on assessment of bony proxies (Antón, 1990; O'Connor et al., 2005). Conversely, O'Connor et al. (2005) estimated generally comparable muscle cross-sectional areas in Pleistocene and recent robust modern humans relative to Neanderthals. When compared to *H. heidelbergensis*, Eng et al. (2013) estimated slightly larger mean temporalis and masseter muscles, but smaller medial pterygoids, in *H. sapiens*. These discrepancies reflect not only differences between populations, but also the significant errors inherent in estimation of muscle cross-sectional areas from bony proxies in humans (Toro-Ibacache et al., 2015).

This traditionally proposed general gracilization of the craniofacial complex (based on samples of more gracile modern humans) led to the view that modern humans produce lower bite forces and are less able to withstand masticatory strains than other hominins (Lieberman, 2011; Zink and Lieberman, 2016). Few studies have compared the biting performance of *H. heidelbergensis* and *H. sapiens*, but *H. heidelbergensis* has been shown to have a masticatory system that is less mechanically advantageous (Spencer and Demes, 1993; Eng et al., 2013). Despite this, it has been proposed that, relative to recent modern humans, *H. heidelbergensis* could generate slightly higher bite forces, absolutely and relative to crown area, at the first molar, and slightly lower bite forces at the first incisor (Lieberman, 2011). Conversely, Eng et al. (2013) estimated clearly higher bite forces at the second molar in Pleistocene and recent modern humans than in *H. heidelbergensis*, absolutely and relative to occlusal area.

Several studies have investigated the masticatory biomechanics of *H. neanderthalensis* (Rak, 1986; Demes, 1987; Trinkaus, 1987a; Demes and Creel, 1988; Antón, 1990; Spencer and Demes, 1993; Antón, 1996; O'Connor et al., 2005; Clement et al., 2012). It has been proposed that Neanderthals were adapted to generate and withstand high and/or repetitive occlusal loads at the anterior dentition (the anterior dental loading hypothesis; Rak, 1986; Demes and Creel, 1988). This has supported the notion that *H. sapiens* is less adapted to generate and withstand high anterior bite forces. However, several studies have found that *H. sapiens* is relatively more efficient at generating bite forces than Neanderthals (Antón, 1990; Spencer and Demes, 1993; O'Connor et al., 2005; Lieberman, 2011). This is because *H. sapiens* has greater muscle mechanical advantages due to its retracted and shorter face and the more anteriorly positioned masticatory muscles (Trinkaus, 1987a; Antón, 1990; O'Connor et al., 2005; Wroe et al., 2010; Lieberman, 2011; Eng et al., 2013; Ledogar et al., 2016a). Modern humans are thought to possess masticatory muscles that are generally smaller (in recent gracile specimens; Antón, 1990; O'Connor et al., 2005) or comparable in cross-sectional area to Pleistocene and recent robust specimens (O'Connor et al., 2005; Eng et al., 2013) and therefore muscle forces. As such, and when considering differences in biting leverage, bite forces estimated for modern humans are comparable to (in Pleistocene and recent robust specimens; O'Connor et al., 2005; Eng et al., 2013) or higher than (in recent specimens; Antón, 1990; Spencer and Demes, 1993; Eng et al., 2013) those calculated for Neanderthals.

While there is some debate about the bite force production capability of these species, it seems that *H. sapiens* is not well adapted to withstand masticatory forces when compared to *H. heidelbergensis*. Thus, the larger face of the latter has been proposed to resist masticatory stresses and strains better than *H. sapiens* (Lieberman, 2011). Likewise, Neanderthals have been said to be better adapted for resisting biting loads than *H. sapiens*, especially during anterior dental loading. This is because Neanderthals present a taller, more inflated and more parasagitally orientated infraorbital region that lacks a canine fossa and large anterior teeth, while modern humans have shorter facial height, a coronally orientated infraorbital region, a canine fossa and smaller anterior teeth (Rak, 1986; Demes, 1987; Lieberman, 2011).

The above studies compared biting performance using lever arm mechanics and simplifications of skeletal facial anatomy, i.e., using two-dimensional diagrams in which the cranium is greatly simplified rather than considering the full three-dimensional (3D) anatomy of the masticatory system. More recently, craniofacial biomechanical studies of biting in hominins have used Finite Element Analysis (FEA; Strait et al., 2007, 2009, 2010; O'Higgins et al., 2011; Witzel, 2011; O'Higgins et al., 2012, Smith et al., 2015; Ledogar et al., 2016b). This approach involves the creation of 3D models of the cranium that are then allocated bone material properties and loaded to simulate muscle attachments, lines of action and forces, with constraints applied at biting points and joints to fix the cranium in space (O'Higgins et al., 2011, 2012). Functional simulations using this approach lead to predictions of bite forces and the stresses and strains experienced by the craniofacial complex. FEA has been used in craniofacial biomechanical analyses of fossil hominins, such as australopiths (Strait et al., 2009, 2010, Wroe et al., 2010; O'Higgins et al., 2011; Smith et al., 2015; Ledogar et al., 2016b, 2017) and *H. neanderthalensis* (Witzel, 2011), but the bite force generation efficiency and skeletal performance in resisting bites of *H. sapiens* have not yet been compared to its proposed ancestor, *H. heidelbergensis*, using FEA.

Thus, the present study assesses the impact of differences in facial size and midfacial retraction found between modern humans and *H. heidelbergensis* on the biting performance of these two species. Based on prior work, it is expected that differences will be found in: (i) bite force efficiency and possibly capability; (ii) the ability to resist deformations arising during masticatory loading; and (iii) the magnitudes and modes of deformation experienced by the craniofacial complex. We consider the implications of our findings in relation to adaptation in the craniofacial skeleton of modern humans. Thus, the reduced midface of *H. sapiens* relative to that of *H. heidelbergensis* (both species represented by proxy

specimens) has mechanical (efficiency of conversion of muscle force into biting force, and load resistance) and, plausibly, morphological consequences (the development of a chin). In particular, we consider if these are adaptive changes or are secondary to other causes of midfacial reduction.

2. Materials and methods

2.1. Materials

Adult crania of *H. heidelbergensis* and *H. sapiens* were compared, in terms of the following mechanical performance parameters that relate to biting: (1) the mechanical advantages of the main jaw adductor muscles (temporalis, masseter and medial pterygoid); (2) the bite forces generated and bite force production efficiency (the proportions of net muscle force converted into bite force and into joint reaction forces); and (3) the magnitudes and modes of deformation of each cranium assessed locally using strains and, globally, using geometric morphometrics.

The calculation of mechanical advantages used two specimens attributed to *H. heidelbergensis*, Broken Hill (also known as Kabwe 1) and Petralona (Greece), both presumed males (Rightmire, 2013). As noted in the Introduction, these come from different continents and so represent populations of archaic *Homo* that may have different phylogenetic histories and fates. However, form rather than phylogeny determines mechanical performance and these fossils are more similar to each other than either is to modern humans (Freidline et al., 2012; Hublin et al., 2017), and so both are considered in the analysis of lever mechanics.

The cranium of *H. sapiens* is that of a 74-year-old male from Hull, England, who gave prior consent for this research as approved under the relevant national legislation (The Human Tissue Act 2004; see Winterton, 2006) and by the relevant Hull York Medical School Ethics committee. The same cadaveric head was previously used by Toro-Ibacache et al. (2016a) for validation of masticatory function. In that study, the head was dissected, segmented, and used to create an FE model that was mechanically loaded to approximate the simulation of an incisor bite. Similarly, Godinho et al. (2017) assessed validity of the cranium in simulated M^1 biting. The cranium was extremely well preserved but bilaterally lacked the upper fourth premolars, with no substantial gaps in the dental arcade. It is used in this study because we understand the limits of its validity and sensitivity to modelling errors better than any other human cranium yet subjected to FEA. The protocol for FEA modelling that we apply to both crania (the human and Broken Hill) in this study was developed using it.

The FEA part of the study does not take account of intraspecific variation because the available CT scan of Petralona is of too low a resolution to reliably build an FEA model. However, the interspecific morphological differences between *H. heidelbergensis* and *H. sapiens* (see above and Freidline et al., 2012; Hublin et al., 2017) are clearly larger than the intraspecific ones, thus mitigating the limitations inherent in studying only one representative per species.

2.2. Mechanical advantages

Mechanical advantages (ratio of forces out to forces in) were calculated for the jaw adductor muscles (temporalis, masseter and medial pterygoid) based on 3D landmarks on two crania of *H. heidelbergensis* (Broken Hill and Petralona) and one cadaveric *H. sapiens* (Fig. 1). Landmarking of Petralona was based on an isosurface of the CT, with no further reconstruction. Landmarking of Broken Hill and the human cranium were based on the full reconstructions of the crania (described below). Petralona and

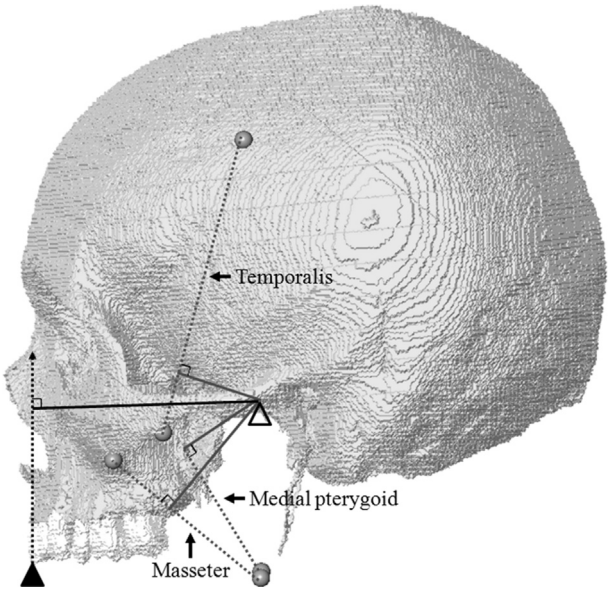

Figure 1. Measurement of muscle in-lever arms (grey solid lines connecting points indicating estimated centres of attachment of temporalis, masseter and medial pterygoid) and the incisor out-lever arm (black solid line) in *Homo sapiens*. The in-lever arms were calculated as the perpendicular distance from the fulcrum to the respective muscle line of action (grey dotted lines). The out-lever arms were calculated according to O'Connor et al. (2005), as the perpendicular distance from the fulcrum to the vector of the bite force applied (black dotted line). The hollow triangle indicates the constraint at the glenoid fossae, where the joint reaction forces (Fc) were calculated; the solid triangle represents the constraint at one of the three different bite points (left central incisor) where the bite force (Fb) was calculated.

Broken Hill lack the lower jaw; thus, to estimate the insertions of masseter and medial pterygoid, a Neanderthal mandible (Tabun 1) was scaled to each of the specimens. Because masseter and, especially, temporalis are muscles with wide origins, the mechanical advantages may vary markedly depending on which point of origin of the muscles is selected. Thus, to bracket the range in each of these two muscles, the mechanical advantages were calculated for their most anterior and posterior points of origin. For temporalis, a third, intermediate, line of action was also defined, approximately in the centre line of the muscle, where it bulges and reaches its most superior point. These anatomical points were easily identifiable due to the presence of muscle scarring. The mechanical advantages of a lateral incisor bite were also calculated for *H. sapiens* and the results were averaged to render them comparable with those of O'Connor et al. (2005), where the mechanical advantages (i.e., in-lever/out-lever) were calculated for the lateral incisor. Even though the sample of *H. heidelbergensis* is small, Broken Hill and Petralona are the best preserved and most complete crania commonly ascribed to this species, thus providing the most reliable and complete data. The mechanical advantages were measured in only one specimen of *H. sapiens*, but the results for temporalis and masseter in this individual were consistent with those from other studies and only slightly higher for medial pterygoid (O'Connor et al., 2005, and see the Results section).

2.3. Bite forces

Bite forces were calculated from the reaction forces at the bite points of the finite element models of the *H. heidelbergensis* (Broken Hill) and *H. sapiens* (cadaveric) specimens. The bite force production efficiency reflects the proportion of net applied muscle force converted into bite force and the proportion that contributes to reaction forces at the fulcrum at the glenoid fossa. These are

calculated as the ratio of the bite force and net muscle force applied (Fb/Fm) and the ratio of the summed reaction forces at the glenoid fossae and net muscle force applied (Fc/Fm; Antón, 1990; O'Connor et al., 2005). The term 'net muscle force' is applied here to the sum of all reaction forces at the constrained nodes on the teeth and glenoid fossa. It differs from the total muscle force due to the orientation of the muscle force vectors. The magnitudes, directions and modes of deformation were calculated from the displacements arising from the FEA (described below).

2.4. Finite element models

The virtual models of Broken Hill and the cadaveric *H. sapiens* were created from CT scans. After segmentation and reconstruction, both models were converted into voxel-based finite element models and were used to simulate three different bites. Because the modern human cranium lacks one of the premolars in the left and right hemiarcades, tooth and bite point correspondence is established in terms of position along the dental arcade rather than by tooth type. This decision was based on a sensitivity analysis in which the effect of replacing the left first molar crown of the *H. sapiens* model with the left premolar crown was negligible; strains in the face did not change, except locally in the crown and alveolus, whereas the effect of varying bite location was marked. In consequence, the simulated bites used the first left tooth (left central incisor in both models), the fourth left tooth (left third premolar in both models) and the fifth tooth (left first molar in *H. sapiens* and left fourth premolar in Broken Hill).

2.4.1. FE model creation

2.4.1.1. Broken Hill. A full description of the reconstruction of the Broken Hill cranium was provided by Godinho and O'Higgins (2017). As such, here we provide a brief summary of the reconstruction of this cranium.

The cranium of Broken Hill was reconstructed (Fig. 2) from a CT scan (courtesy of the Natural History Museum, London), with an original anisometric voxel size (0.4687501 × 0.4687501 × 0.50 mm), that was resampled to an isometric voxel size of 0.35 mm. Automated, semiautomated and manual segmentation to refine fine details were performed using Avizo® version 7.0 (Visualization Sciences Group). This was followed by reconstruction of the missing anatomical regions of the cranium, such as the right temporal, parts of the right parietal, occipital, maxillae, ethmoid and teeth. Where possible, this was achieved by mirroring present contralateral anatomical areas and warping them to the existing structures. Geomagic® (Studio 2011) was used to fill small gaps using the surface of surrounding structures as a reference for interpolation. When no contralateral structures were present in Broken Hill, portions of the *H. sapiens* cranium (portion of the occipital bone and crowns of teeth) were also used for reconstruction, by warping them to fit. The cancellous bone spaces were infilled with material to form a bulk material (see below).

2.4.1.2. Homo sapiens. The cranium of *H. sapiens* was originally segmented by Toro-Ibacache et al. (2016a) based on a CT scan of a cadaveric human head with an original isometric voxel size of 0.484 mm that was later resampled to an isometric voxel size of 0.350 mm. Automated, semiautomated and manual segmentation of the skeletal structures was performed and cortical bone, cancellous bone (as a bulk material) and teeth were originally segmented as separate materials. The cranium was then directly converted into a voxel-based finite element model using a bespoke software tool, vox2vec. It was submitted to validation studies that simulated incisor (Toro-Ibacache et al., 2016a) and molar bites (Godinho et al., 2017), as well as a sensitivity study assessing the impact of model simplification on performance (Toro-Ibacache et al., 2016a; Godinho et al., 2017).

On the basis of these sensitivity studies, and the study of Fitton et al. (2015), which show a marked effect on magnitude, but a very small effect on mode of deformation, both models were simplified by filling cancellous bone regions with material that has the same material properties as cortical bone and allocating the same cortical bone properties to teeth (see Material properties, below). This allowed comparability with the Broken Hill FE model, which is simplified of necessity, because the CT scan lacks detail of cancellous bone architecture and distribution (see below).

2.4.2. Constraints

Similar constraints were applied to the models of Broken Hill and *H. sapiens* using the finite element analysis software tool VoxFE (Fagan et al., 2007). Both temporomandibular joints (TMJ) were constrained at 24 nodes (x, y and z axis) and a third constraint (21 nodes, fixed in the z axis) was applied at the simulated bite point in each of the masticatory simulations. Experiments in which one axis of constraint was removed from one of the TMJ resulted in the model rotating when loaded, as such these are the minimum constraints we could apply.

2.4.3. Material properties

Sensitivity studies conducted using the cranium of *H. sapiens* (Toro-Ibacache et al., 2016a; Godinho et al., 2017) show that progressively simplifying the model, from the original three materials (cortical bone, cancellous bone and teeth) with distinct material properties, to a model with one material with properties of cortical bone has a significant effect in reducing the magnitude of strains and of global deformation with a much more limited effect on mode of deformation (relative strain magnitudes between regions and mode of global changes in size and shape). Allocating to teeth the material properties of cortical bone rather than enamel has a very localized effect in the alveolar region, altering magnitude of deformation and less so the mode of deformation (Lacruz et al., 2015; Godinho et al., 2017). These results are consistent with other studies using non-

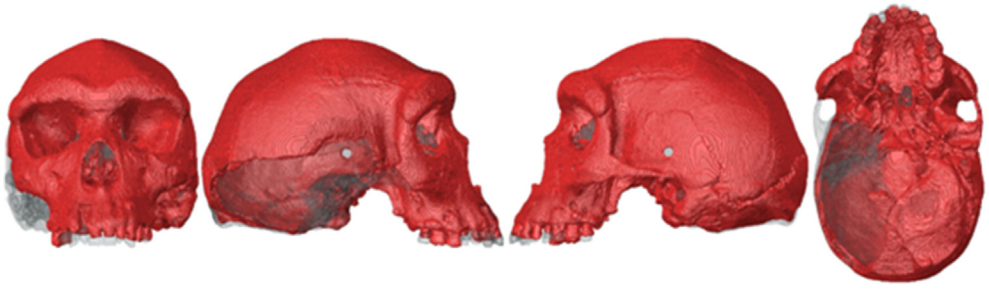

Figure 2. Reconstruction of the Broken Hill cranium. Red areas represent structures originally present and translucent grey represents reconstructed anatomical structures. (For interpretation of the references to color in this figure legend, the reader is referred to the Web version of this article.)

human primates (Fitton et al., 2015) and show that using a one material model should not yield unreliable results in terms of mode of deformation, although magnitude is likely diminished to an unknown degree. Further, this simplification resulted in only a 0.1% increase in the estimated bite force.

This simplification is useful in the current study (Broken Hill) and in other contexts, since fossils often lack anatomical regions because of postmortem damage and are filled with sedimentary matrix, precluding reliable reconstructions of anatomical details, such as the distribution and architecture of cancellous bone (Fitton et al., 2015). By building a one material model, reconstruction is facilitated, yet useful information can still be obtained regarding mode and relative, but not absolute, magnitude of deformation. Such models were created for both *H. sapiens* and Broken Hill, to which cortical bone material properties were allocated, with a Young's modulus of 17 GPa and Poisson's ratio of 0.3. The modulus of elasticity was derived from nanoindentation studies of cortical bone from the skull of *H. sapiens* (Toro-Ibacache et al., 2016a) and is within the range of previous studies (Dechow et al., 1993; Schwartz-Dabney and Dechow, 2003). Since these models are made using the same protocol with regard to segmentation and material properties, we can directly compare deformations and so the strains developed in them—although, as noted above, we cannot confidently predict the absolute magnitudes of deformation. This said, our prior sensitivity studies (Toro-Ibacache et al., 2016a; Godinho et al., 2017) indicated that the relative strains within and between crania provide a good approximation to in vitro simulations of masticatory function. This expectation is further supported by comparison of the strain maps in this study with those previously obtained by Ledogar et al. (2016a) and Toro-Ibacache (2014; see Discussion).

2.4.4. Muscle loads Loads were applied directly to the nodes of the voxel elements that lie in the regions of muscle attachment in our FE models to represent the maximal actions of six muscles active during biting: right and left temporalis, right and left masseter, right and left medial pterygoid. Details of applied forces are given in Table 2. The applied forces were the same in both biting simulations. These are not physiological, because, in life, relative muscle activations change between bite points, and within and between chewing cycles. However, by keeping the forces constant among models, we can control the experiment carefully, modifying just one variable between biting simulations, the bite point. As such, we can directly compare deformations between bites in the knowledge that input forces have not changed. The *H. sapiens* cadaveric head had all the masticatory muscles preserved, as well as the mandible. Thus, it was possible to accurately represent the specimen-specific muscle vectors and muscle forces as estimated from the muscle cross-sectional areas using the CT scans of the head and not from bony proxies (Toro-Ibacache et al., 2016a).

Broken Hill does not have a mandible, which precludes direct estimation of the lines of action and anatomical cross-sectional areas (and so maximum forces) of muscles that attach to the mandible (masseter and medial pterygoid). In the present study, we apply the same muscle forces as in the human to compare the effects of differences in muscle vectors and lever arms on performance rather than the effects of varying input forces. As such, we applied the muscle forces estimated for the *H. sapiens* specimen to Broken Hill. Because Broken Hill lacks a mandible and neither CT scans nor casts of any other *H. heidelbergensis* mandible (e.g. the Mauer mandible) were available, we estimated the directions of muscle force vectors by scaling a mandible of *H. neanderthalensis* (Tabun 1) to the Broken Hill cranium and using it to guide estimation. While this clearly is not the right mandible, this scaling removes the size differences between the cranium and the Tabun mandible thus providing a suitable first approximation of muscle vectors when scaled to fit this cranium. It raises the question, however, of the extent to which error in the estimation of muscle vectors will impact our findings due to the effects of, e.g., allometry. Several prior sensitivity studies (Ross et al., 2005; Bright and Rayfield, 2011; Fitton et al., 2012; Toro Ibacache et al., 2016a,b) have noted that varying muscle vectors or relative forces (which affects net vectors) has relatively little impact on mode of deformation and so on the distribution of regions of relatively high or low strains, although the magnitudes of strains tend to vary with total applied muscle force (which is a constant in our study).

To ensure these findings apply in the present study, we carried out a further sensitivity analysis in which we varied muscle vectors applied to the Broken Hill model. In this sensitivity analysis, we focused on incisor biting, in which strains are greatest. We varied the lines of action of the three muscles on both sides with respect to

Table 1
Landmarks used for extraction and plotting of strains (landmarks 1–41; midline and left sided) and for GM analysis of magnitudes and modes of deformation (landmarks 1–67, with 42–67 being right sided).

Number	Landmark
1	Bregma
2	Lambda
3	Inion
4; 42	Asterion
5; 43	Porion
6; 44	Pterion
7; 45	Frontomalare orbitale
8; 46	Frontomalare temporale
9; 47	Jugale
10; 48	Zygotemporale superior
11; 49	Zygotemporale inferior
12; 50	Maxillofrontale
13; 51	Zygoorbitale
14; 52	Zygomaxillare
15; 53	Superior rim of orbit
16; 54	Infraorbital foramen
17	Nasion
18	Rhinion
19; 55	Lateral Nasal Suture
20	Nasospinale
21; 56	Alare
22	Alveolare
23; 57	External Alveolar Incisor 2
24; 58	External Alveolar Canine
25; 59	External Alveolar Premolar4
26; 60	Zygomatic take-off
27; 61	Inferior Distal Alveolar
28	Incisive Foramen
29	Palate maximum
30	Staphylion
31; 62	Infratemporal crest
32	Basion
33	Opisthion
34; 63	Lateral edge of foramen magnum
35	Hormion
36	Glabella
37	Supraglabella
38; 64	Inferolateral choanal corner
39; 65	Anterior edge of anterior ethmoid foramen
40; 66	Posterior edge of posterior ethmoid foramen
41; 67	Inferiormost margin of nasal aperture

Table 2
Applied muscle forces (in newtons, N).

	Left	Right
Temporalis	168.02	170.67
Masseter	134.06	124.01
Medial pterygoid	124.01	117.49

lines estimated from the Tabun mandible, such that the vectors are directed more anteriorly by 5°, more posteriorly by 5°, more laterally by 5°, and more medially by 5°. The impact on the magnitudes and distributions of strains is low to negligible. Anterior rotation causes a slight increase (~5%) in strains, posterior rotation a slight decrease (~5%) and mediolateral rotation has even a lower impact (~2%).

In summary, while another *H. heidelbergensis* mandible such as the Mauer mandible would have better served estimation of the orientations of muscle vectors of the Broken Hill cranium, using such a mandible would still raise issues of suitability, because of intraspecific variation. Neither is the use of the Tabun mandible ideal. Therefore, after scaling the mandible to obtain an estimate of muscle vectors we assessed the impact of error in these estimates by performing the sensitivity analysis described above. Our results show that changing the orientation of the muscle vectors by 5° mediolaterally and anteroposteriorly has limited impact. This range likely incorporates the true vectors and shows that the results of FEA differ little throughout the whole range of likely muscle vectors. This gives us confidence that our results are not unduly affected by errors in muscle vectors applied to the FE model.

2.4.5. Model solution and analysis The FE models were solved using VoxFE (Fagan et al., 2007). The resulting deformations of the two models were then compared by: (1) visual assessment of contour plots of the two surface principal strains ($\varepsilon 1$ and $\varepsilon 3$; maximum and minimum principal strains) magnitudes over the whole cranium and of strain vector directions over the infraorbital plate; (2) quantitative comparisons of the surface strain magnitudes experienced at 67 homologous points, of which the magnitudes at 41 points from the midline and left side of the cranium were plotted for comparison (loading is on the left and so the largest strains are developed on this side in that bite; see Table 1); and (3) comparisons among the loaded models of modes of global deformation (changes in size and shape) relative to the unloaded mean (of the modern human and Broken Hill) specimen using geometric morphometric (GM) analyses of the full set of 67 midline and bilateral cranial landmarks (see Table 1).

In the GM analysis, the landmark coordinates differ between the unloaded and loaded models of *H. sapiens* and *H. heidelbergensis* because of differences in size, translation, rotation, cranial shape and, in the case of loaded models, deformation (mode and magnitude of change in cranial shape due to loading). We are only interested in the last, the effects of loading, which are very small compared to the differences in size and shape between unloaded models. Since loading results in changes in both size and shape, we consider them jointly by first undertaking a generalized Procrustes analysis (GPA) of all unloaded and loaded crania to account for the effects of differences in size, translation and rotation. This results in shape variables which are the GPA registered coordinates. Next, size is reintroduced (see Supplementary Online Material (SOM) S1) by multiplying the shape coordinates of each loaded and unloaded model by its original centroid size. This results in size and shape coordinates for each model. The differences in size and shape coordinates calculated between the unloaded and loaded models (loaded minus unloaded coordinates) describe the deformations of each model rather than the sizes and shapes of models. Note that here 'deformation' means changes in size and shape calculated as above, rather than raw displacements of landmarks between unloaded and loaded models. The raw displacements can include rigid body motions that do not concern us.

To visualize and compare deformations as changes in size and shape of each cranium, we follow the approach set out in a series of previous papers (O'Higgins et al., 2011, 2012; Milne and O'Higgins, 2012; O'Higgins and Milne, 2013). Thus, the differences in size and shape coordinates (after scaling to account for differences in, e.g., size, forces, etc., as required, see below) were added to the coordinates of an unloaded cranium to facilitate visualization of results. The choice of unloaded cranium does not impact the distances computed among model deformations or the subsequent principal components analysis (PCA). Here we choose the mean unloaded cranial size and shape coordinates (of Broken Hill and the specimen of *H. sapiens*) for this purpose. The mean unloaded cranial size and shape is calculated by multiplying the mean shape coordinates of the unloaded crania (from the initial GPA) by the mean centroid size of the unloaded crania. This entire maneuver results in new representations of loaded crania, as deformed versions of the mean cranial size and shape. Finally, to visualize the modes and magnitudes of deformation, a PCA is carried out (with no further GPA) of the mean unloaded cranial size and shape together with the new representations of the loaded crania referred to the mean.

2.4.6. Scaling It is not possible to directly compare absolute bite force generation capacity between the modern human and Broken Hill, because no direct data are available on the cross-sectional areas of masticatory muscles in the latter. Thus, we focus on a comparison of biting efficiency (of conversion of muscle to bite forces), applying the same muscle forces to the modern human and Broken Hill crania in all FEA biting simulations. However, for completeness, further analyses are carried out that take account of possible differences in applied and reaction forces and of differences in facial size.

To account for potential differences in applied muscle forces, it was necessary to scale the results of FEA according to our best estimate of masticatory muscle cross-sectional areas and so, forces. This estimate is obtained using the cross-sectional area of the left temporal fossa, a bony surrogate for temporalis cross-sectional area and, because of the lack of mandibles, the only bony proxy available for the masticatory muscles. Its validity depends on the validity of two assumptions: that temporal fossa area predicts muscle cross-sectional area (which it likely does not; see Toro-Ibacache and O'Higgins 2016); and that there exists a similar relationship among the cross-sectional areas of the different masticatory muscles in the two individuals. As such, it is a crude estimate, but the best we can make.

To estimate actual performance in Broken Hill, the degree of deformation it would have undergone if (estimated) actual muscle forces had been applied, principal strains are scaled according to the ratio of applied and estimated actual muscle forces. Likewise, to account for differences in bite forces between the modern human and Broken Hill, the principal strains and size and shape distances (GM analysis) are scaled according to the ratio of bite forces. These scalings rely on the fact that deformations (strains and global changes in size and shape, as assessed by the GM analysis) scale linearly and with a slope of 1, with applied forces (Milne and O'Higgins, 2012; O'Higgins and Milne, 2013).

To account for differences in facial size between the modern human and Broken Hill, the strains experienced by Broken Hill were scaled according to the inverse of the ratio of facial surface areas. This is because stress is the result of a force applied over an area ($\sigma = F/A$) and strain ($\varepsilon = \Delta l/l$) scales with stress, through Hooke's law (extension is proportional to applied force) within the elastic limits of homogenous, isotropic materials (Bird and Ross, 2012).

Although scaling of stresses and strains to account for size differences is well understood (Dumont et al., 2009), the scaling of size and shape distances in GM analysis due to size differences (as described above) is not. SOM S1 demonstrates that the size and shape distances between loaded and unloaded models of the same shape scale inversely with lengths (such as the square root of area, or centroid size). As such, the deformations (differences in size and shape coordinates) occurring in differently sized FEA models can be scaled to account for size differences prior to comparison,

according to the inverse of the ratio of their centroid sizes. It is worth noting that this scaling is approximate, because differences in magnitudes of deformation arise when size is varied but differences in modes of deformation arise when shape is varied (SOM S1). This means that scalings between *H. heidelbergensis* and *H. sapiens* are inevitably approximations, whose validity is a function of the degree of difference in shape between them. A similar caveat applies to scaling of strains (e.g., Grosse et al., 2007) and of muscle forces, since their vectors will vary with shape.

Thus, to compare performance while simultaneously accounting for differences in facial size and applied or biting forces, we used two different scalings. First, we scaled the deformations of Broken Hill for differences between the two specimens in facial size and in applied muscle forces by scaling the strains according to the inverse of the ratios of facial surface areas (in the FEA analysis of principal strains), or to the inverse of the ratio of facial centroid sizes (in the GM analysis of size and shape differences), and the ratio of temporalis cross-sectional areas. These scalings allow us to compare deformations in Broken Hill and *H. sapiens* accounting for differences in facial size and applied muscle forces. Second, we scale the deformations according to the inverse of the ratios of facial areas or centroid sizes (as in the previous scaling) and the ratio of bite reaction forces. This allows us to compare Broken Hill to *H. sapiens* accounting for differences in facial size and bite forces.

3. Results

3.1. Mechanical advantages

The estimated mechanical advantages are presented in Table 3. Petralona and Broken Hill present similar mechanical advantages that increase, as expected, from anterior to posterior bites, due to shortening of the out-lever arm (length of the resistance arm) while the in-lever arm (lengths of the muscle effort arms) remains constant. The mechanical advantages (MA) of the cadaveric *H. sapiens* are within the range of or, in the case of medial pterygoid, slightly greater than in the male sample presented by O'Connor et al. (2005) for lateral incisor biting (the only bite point calculated in that study). The maximum value for temporalis MA in O'Connor et al. (2005) is 0.307 and the mean value in the individual included in the study is 0.281; for masseter, maximum value in O'Connor et al. (2005) is 0.484, mean value in this individual is 0.4836; medial pterygoid, maximum value in O'Connor et al. (2005) is 0.469, value in this individual is 0.533. At the remaining bite points used in this study, mechanical advantages increase from anterior to posterior bites, with *H. sapiens* always presenting greater values than Broken Hill and Petralona. Thus, the *H. sapiens* specimen is more efficient at converting muscle forces into bite forces (Table 3), and results in ratios of the mechanical advantages of Broken Hill/*H. sapiens* and Petralona/*H. sapiens* which are always less than 1 (Table 4).

3.2. Bite forces and force production efficiency

When the same muscle forces are applied, the ratio of bite forces predicted for Broken Hill to those predicted for *H. sapiens* is 0.51–0.55 (Table 5). Scaling for possible differences in muscle areas and, therefore, muscle forces using the surface area of the temporal fossa as a proxy (ratio Broken Hill/modern human estimated to be 1.18), results in smaller bite force differences, although Broken Hill still generates lower bite forces than *H. sapiens* (ratios = 0.60–0.65). Thus, as expected, force production efficiency is lower in Broken Hill than in the *H. sapiens* model, with the ratio of bite forces to net applied muscle forces in Broken Hill being 0.35–0.45, while in *H. sapiens* the ratio is 0.46–0.65. In consequence, the ratio of the joint reaction forces to net applied muscle forces is larger in Broken Hill (0.55–0.65) than in *H. sapiens* (0.35–0.54; Table 6).

3.3. Strains

Again, as expected, because of differences in size and robusticity, principal strain contour plots for the two models (Fig. 3) show that *H. sapiens* experiences significantly higher strains than those that arise in Broken Hill when the same muscle forces are applied. The difference is reduced after scaling principal strains according to the inverse of the ratio of facial surface areas and the ratio of muscle forces, although the scaled Broken Hill strains are still lower than in *H. sapiens*. When scaling the strains of Broken Hill according to the inverse of the ratio of surface areas of the face and the ratio of bite forces, the strains become generally comparable. The strain contour plots show that, in both *H. heidelbergensis* and *H. sapiens*, the largest strains are found in generally similar anatomical areas, such as directly above the bite points, the zygoma, the postorbital bar and

Table 3
Mechanical advantages of the main masticatory muscles in *Homo heidelbergensis* (Broken Hill, Petralona) and *Homo sapiens*.

	Bite point	Temporalis (anterior)	Temporalis (middle)	Temporalis (posterior)	Masseter (anterior)	Masseter (posterior)	Medial pterygoid
Broken Hill	I^1	0.31	0.19	0.06	0.37	0.22	0.37
	P^3	0.39	0.24	0.08	0.47	0.28	0.47
	P^4/M^1	0.42	0.26	0.09	0.51	0.31	0.52
Petralona	I^1	0.28	0.20	0.07	0.35	0.25	0.36
	P^3	0.35	0.25	0.08	0.43	0.31	0.45
	P^4/M^1	0.38	0.27	0.09	0.47	0.33	0.49
Homo sapiens	I^1	0.34	0.33	0.12	0.56	0.34	0.50
	P^3	0.43	0.43	0.15	0.73	0.44	0.64
	P^4/M^1	0.50	0.49	0.18	0.84	0.51	0.74

Table 4
Ratios of the mechanical advantages of the main masticatory muscles in *Homo heibelbergensis* (Broken Hill, Petralona) and *Homo sapiens*.

	Bite point	Temporalis (anterior)	Temporalis (middle)	Temporalis (posterior)	Masseter (anterior)	Masseter (posterior)	Medial pterygoid
Broken Hill / *H. sapiens*	I^1	0.91	0.57	0.52	0.66	0.64	0.75
	P^3	0.89	0.56	0.51	0.65	0.63	0.74
	P^4/M^1	0.85	0.53	0.48	0.62	0.60	0.70
Petralona / *H. sapiens*	I^1	0.84	0.61	0.56	0.62	0.72	0.73
	P^3	0.80	0.58	0.54	0.59	0.69	0.70
	P^4/M^1	0.76	0.55	0.51	0.56	0.66	0.66

Table 5
Bite reaction forces generated by *Homo heidelbergensis* (Broken Hill) and *Homo sapiens* FE models. Unscaled, assuming identical muscle cross-sectional areas and scaled using larger cross-sectional areas to account for the larger area of the temporal fossa in Broken Hill (see text). The last row presents the ratio of bite forces between the unscaled Broken Hill model and that of *H. sapiens*.

Specimen	Bite point		
	I^1	P^3	P^4/M^1
Broken Hill (unscaled)	184.29	219.59	241.37
Broken Hill (scaled for surface area of temporal fossa)	217.24	258.86	284.53
Homo sapiens	332.60	404.29	477.23
Ratio (Broken Hill unscaled / *H. sapiens*)	0.55	0.54	0.51

Table 6
Force production efficiency calculated from the finite element models of *Homo heidelbergensis* (Broken Hill) and *Homo sapiens*.

Specimen (bite point)	Force production efficiency	
	Fb/Fm	Fc/Fm
Homo sapiens (left I^1)	0.46	0.54
Homo sapiens (left P^3)	0.56	0.44
Homo sapiens (M^1)	0.65	0.35
Broken Hill (left I^1)	0.35	0.65
Broken Hill (left P^3)	0.41	0.59
Broken Hill (left P^4)	0.45	0.55

Fb, bite force; Fc, joint reaction forces; Fm, Total muscle force.

the pterygoid fossae. Despite these similarities, the interorbital region and browridges of *H. sapiens* manifest higher strains than Broken Hill (Fig. 3). Similarly, Broken Hill experiences proportionally (not absolutely) higher strains in some anatomical regions (e.g., body of the zygomatic) than *H. sapiens*.

The strains at the 41 landmarks (Fig. 4) reflect the findings of Figure 3. Thus, when the same muscle forces are applied, Broken Hill experiences lower strains than the *H. sapiens* model (left hand column of plots). After scaling for differences in muscle force and facial surface areas (middle column), differences between specimens decrease, but are still generally lower in Broken Hill than in the modern human. After scaling for bite force and facial surface areas (right column), differences between the models decrease markedly and become generally comparable (see SOM Table S1 for details on exact strain magnitudes). The pattern of variation among landmarks in strain magnitudes is generally similar between the two models, although some regions experience relatively higher strains in one model than in the other (Fig. 4 and SOM Table S1). Thus, our FE models of Broken Hill and *H. sapiens* experience generally similar modes of deformation, albeit with some differences. However, magnitudes of deformation differ markedly before scaling according to the inverse of the ratio of facial areas, muscle forces and bite forces (Fig. 3).

Figure 5 shows that, despite some similarities, the directions of the maximum ($\varepsilon 1$) and minimum ($\varepsilon 3$) principal strain vectors differ between the models in the different simulated bites. Over the infraorbital region, vector directions are more regular in Broken Hill than in the modern human. In part, this further indicates differences in modes of deformation and, in part, this is due to its more inflated and more even surface morphology.

3.4. Magnitudes and modes of global deformation

In the size and shape analysis of global deformations (Fig. 6), *H. sapiens* and *H. heidelbergensis* present different magnitudes and modes of deformation, with *H. sapiens* generally deforming more than *H. heidelbergensis* (larger distances from the mean unloaded cranium). The modern human cranium consistently presents lower PC1 (70% of variance) values and higher PC2 (19% of variance) and PC3 (9% of variance) values than Broken Hill, in equivalent bites, with no overlap between the two specimens (Fig. 6A). Warping from the unloaded cranium to the loaded crania (insets of Fig. 6A) shows that loading the central incisor causes the anterior palate to displace superiorly, resulting in shortening and widening of the nose and orbits, as well as inferomedial deflection of the zygomatic arches. The third premolar bite causes inferomedial deflection of the zygomatic arches and rotation of the palate, together with the lateral margin of the nose, towards the working side (left). This results in an asymmetry between the working and balancing sides of the cranium visible in the shorter and wider left orbit. The first molar/fourth premolar bite results in deformations similar to those in the third premolar bite, with a more posterior location of the point about which deflection of the dental row occurs (Fig. 6A). Figure 6B shows differences in deformation during the same simulated bites in Broken Hill (reference) and the modern human (target). Since these diagrams show differences in deformation they should be read as follows: relative to Broken Hill, the modern human presents more inferior deflection of the zygomatic arches in posterior biting and greater deformation of the external aspect of the nasal cavity (less so in anterior bites). In the first incisor bite, *H. sapiens* develops less anterior displacement of the subnasal region (seen as a relative inferoposterior deformation of the grid). In P^3 and P^4/M^1 bites, the *H. sapiens* cranium also shows more rotation/deformation of the palate about the anteroposterior axis, i.e., more vertical displacement of the working side (seen in the higher position of the canines and in the superior deflection of the transformation grid in this region).

4. Discussion

4.1. Mechanical advantage

The present comparisons of mechanical advantages and force production efficiencies show that the specimen of *H. sapiens* is more efficient at converting muscle force into bite force than the two fossils attributed to *H. heidelbergensis*. This is because the modern retracted and orthognathic face shortens the bite out-lever relative to the muscle in-lever arms of *H. heidelbergensis*, consistent with previous findings by Eng et al. (2013). This is similar to reports from previous studies comparing *H. sapiens* and *H. neanderthalensis* (Antón, 1990; O'Connor et al., 2005; Eng et al., 2013) and parallels findings in modern humans with orthognathic versus prognathic faces (Toro-Ibacache et al., 2016b). The finding of similar jaw lever mechanics in the African (Broken Hill) and the European (Petralona) crania reflects similarities in overall cranial morphology shown metrically by Baab and McNulty (2009) and Hublin et al. (2017). Similarities in craniofacial form and masticatory system functional morphology suggest that these crania will perform similarly in FEA but this requires testing in future work.

We found that a greater proportion of muscle force is consistently converted into bite reaction forces and less into reaction forces at the glenoid fossae in the specimen of *H. sapiens* than in Broken Hill. It is worth noting in this regard that Ledogar et al. (2016a) found that modern humans have high biting leverage, but that they experience tensile joint forces at the working side. This led them to conclude that high biting leverage in humans could be an evolutionary by-product or spandrel, which the current study also concludes (along with Lieberman, 2011; see later in Discussion).

Consistent with Eng et al. (2013), we show that the predicted bite forces of this specimen of *H. sapiens* are considerably higher than those for Broken Hill. Thus, when the same muscle forces are

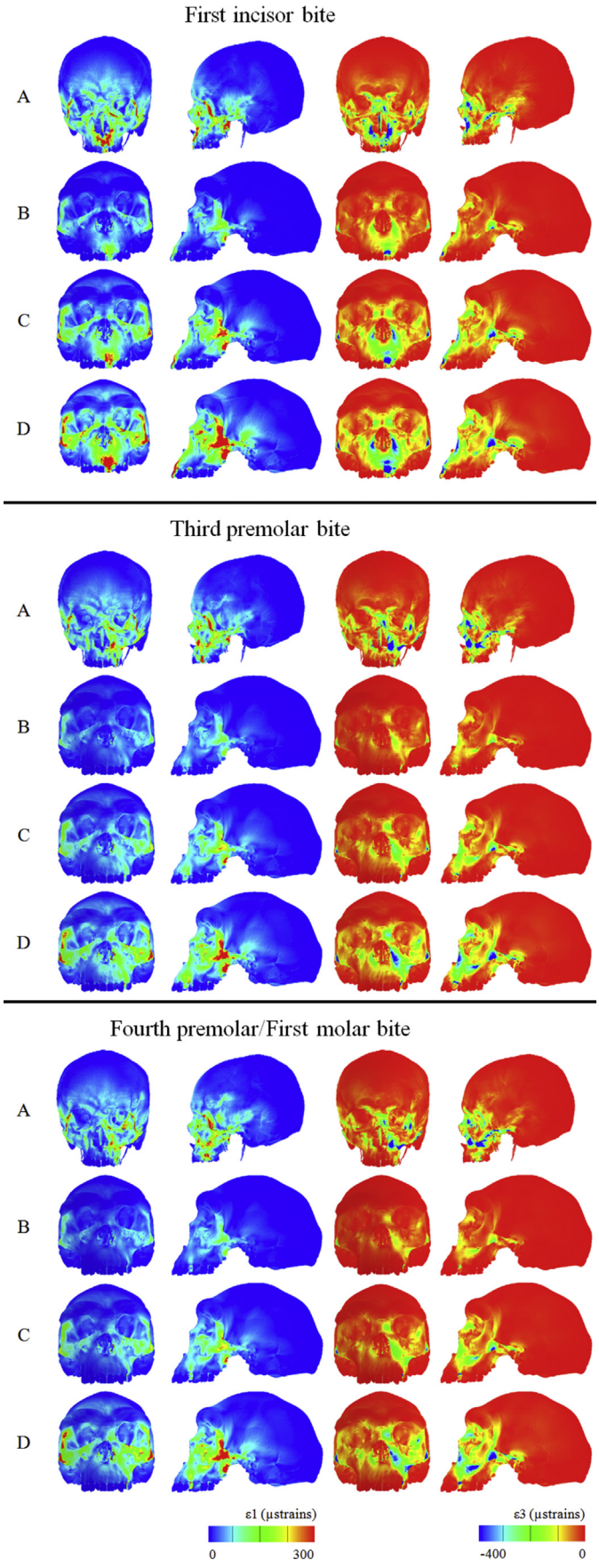

applied, the bite forces estimated for the specimen of *H. sapiens* range from 332.60 N to 477.23 N, 80%–98% greater than those estimated for Broken Hill, which range from 184.29 N to 241.37 N. These comparisons do not take into account differences in muscle forces that may have existed between *H. heidelbergensis* and *H. sapiens*. To do so, the muscle forces in Broken Hill need to be estimated. However, as noted earlier, this can only be done crudely based on scaling of the forces in *H. sapiens*, with the assumptions that temporal fossa area predicts muscle cross-sectional area (which it likely does not, see Toro-Ibacache et al., 2015) and that a similar relationship is present among the cross-sectional areas of the different masticatory muscles in the two individuals (Demes and Creel, 1988). This noted, the surface area of the temporal fossa in Broken Hill is greater than in *H. sapiens* by 18%, suggesting that the temporalis in Broken Hill has the potential to generate bite forces about 18% higher than modelled (but see Toro-Ibacache et al., 2015). Potential errors in estimating the temporalis anatomical cross-sectional area (including inability to take account of pinnation), together with the larger than average medial pterygoid mechanical advantage in the modern human when compared to the data presented by O'Connor et al. (2005), likely impact on the estimates derived here for the differences in predicted bite forces between *H. heidelbergensis* and *H. sapiens*. However, even when considering these differences, our simulation of Broken Hill biting generates bite forces that are lower than those of *H. sapiens*. The ratio of bite forces (Table 5) between the unscaled Broken Hill model and that of *H. sapiens* is similar at the most anterior (~0.55) and at the most posterior bite point (0.51).

Thus there is little evidence from these analyses that Broken Hill was able to generate bite forces that are higher than those in the modern human. This result is interesting in relation to molar crown area as it has been claimed to correlate with bite force (Demes and Creel, 1988). Additionally, Laird et al. (2016) found that reduced occlusal surface area is associated with reduced masticatory efficiency. However, Eng et al. (2013) showed that extant and extinct *Homo* fall below the trend of extant non-human primates and australopiths: they have smaller crown areas than would be expected from their predicted bite forces. Based on direct measurements of the first two (reconstructed) molars, crown areas of Broken Hill are approximately 20% greater than in the *H. sapiens* model and so might be expected to reflect greater rather than smaller bite forces relative to modern humans. This increased bite force relative to molar occlusal area in modern humans derives from our relatively shorter and more orthognathic face, which increases masticatory efficiency (i.e., proportion of masticatory muscle force converted into bite force).

4.2. Craniofacial skeletal performance during biting

Our findings indicate that the facial skeleton of Broken Hill is much less strained during biting than that of the modern human. This stands in contrast to the finding that the modern human is more efficient at generating bite forces and may well have generated a larger bite force than the Broken Hill individual. The predicted lower strain magnitudes in the face of Broken Hill arise not only because of lower muscle and bite forces but also because of size differences. As previously reported, the face of Broken Hill is significantly bigger (about 45%, in surface area) than the face of *H. sapiens* (Freidline et al., 2012). When strains were scaled

Figure 3. Strain contour plots of the solved FE models *Homo heidelbergensis* (Broken Hill) and *Homo sapiens*: A) *H. sapiens*; B) Broken Hill with strains unscaled; C) Broken Hill with strains scaled according to muscle force and size (facial surface area) differences; D) Broken Hill with strains scaled according to bite force and size (facial surface area).

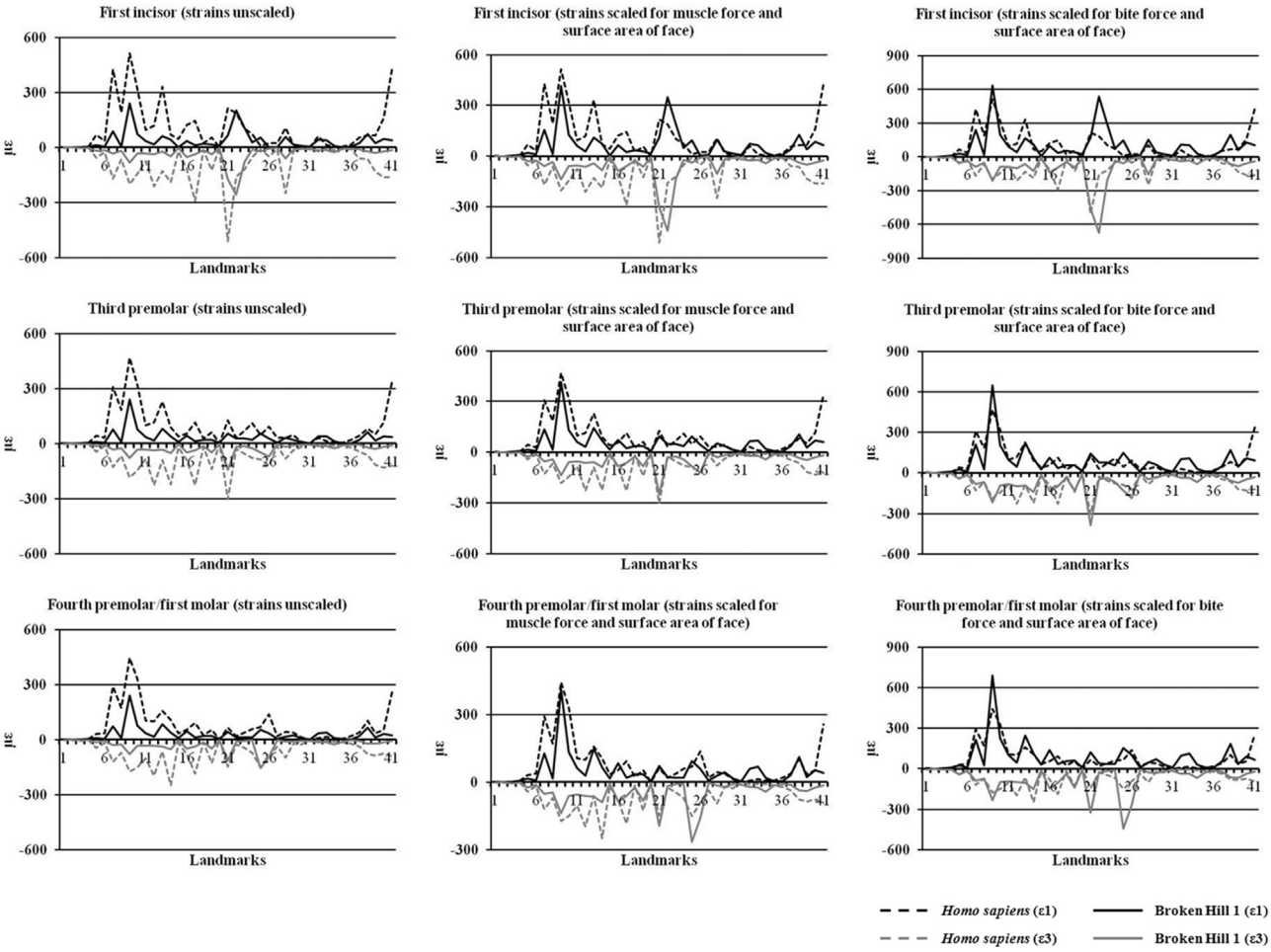

Figure 4. Strains experienced by the FE models at the 41 sampling points: first row, incisor bites; second row, premolar bites; third row, fourth premolar/first molar bites. First and third principal strains are shown (positive and negative values in each plot, respectively). In the left hand column, the strains are unscaled; in the middle column, the strains over Broken Hill were scaled to account for differences in muscle forces and surface areas of the face; in the right hand column the strains over Broken Hill were scaled to account for differences in bite forces and surface areas of the face.

according to the inverse of the ratio of facial surface areas and muscle forces the discrepancies between Broken Hill and *H. sapiens* were reduced but strain magnitudes were still greater in *H. sapiens*. Thus, even accounting for size, and possible differences in muscle forces, Broken Hill resisted biting forces better than *H. sapiens.* In contrast, when strains were scaled according to the inverse of the ratio of facial surface areas and predicted bite forces (see Table 5; bite forces approximately 54% of those developed by the *H. sapiens* specimen) the discrepancies between Broken Hill and *H. sapiens* were markedly reduced and strains become generally comparable (Fig. 4). This is, however, an extreme adjustment; the muscle forces required to achieve identical bite forces are not consistent with the measured temporal fossa area and the face of Broken Hill is in reality much larger than that of the modern human.

These scaling studies reinforce the previous findings suggesting that the Broken Hill cranium is relatively stiffer than would be expected for a modern human of similar facial surface area, and so is better able to resist muscle and biting forces. This is likely due to the generally robust skeleton of Broken Hill and to architectural differences similar to those reported between *H. sapiens* and Neanderthals as being linked to resisting dental loading (Rak, 1986; Demes, 1987). These include the taller subnasal and infraorbital regions found in Broken Hill, and the more sagittally orientated and convex infraorbital plate. These morphological differences may well also be related to the differences found in strain directions.

The GM size and shape analysis of global magnitudes and modes of deformation (Fig. 6) shows that *H. sapiens* deforms differently and to greater degree than Broken Hill, even when accounting for actual differences in facial size and possible differences in bite force. This is consistent with the strain contour plots and graphs (Figs. 3 and 4), which show differences in which regions experience high and low strains, with differences in strain vector directions (Fig. 5).

4.2.1. Significance of apparent differences between Broken Hill and a single modern human The present study examines only two individuals and so it is necessary to consider the extent to which the findings can be generalized to populations. Our findings with regard to differences in masticatory lever mechanics and bite force production efficiency between the modern human and Broken Hill are consistent with those of previous studies and so are unlikely to be due to sampling error.

Similarly, our findings with respect to FEA reflect and extend those of other recent studies. Thus, in an FEA analysis simulating third upper premolar and second molar biting, Ledogar et al. (2016a) compared seven recent human crania from a wide geographic range. They found that, despite intraspecific morphological differences, the crania resisted biting similarly. The

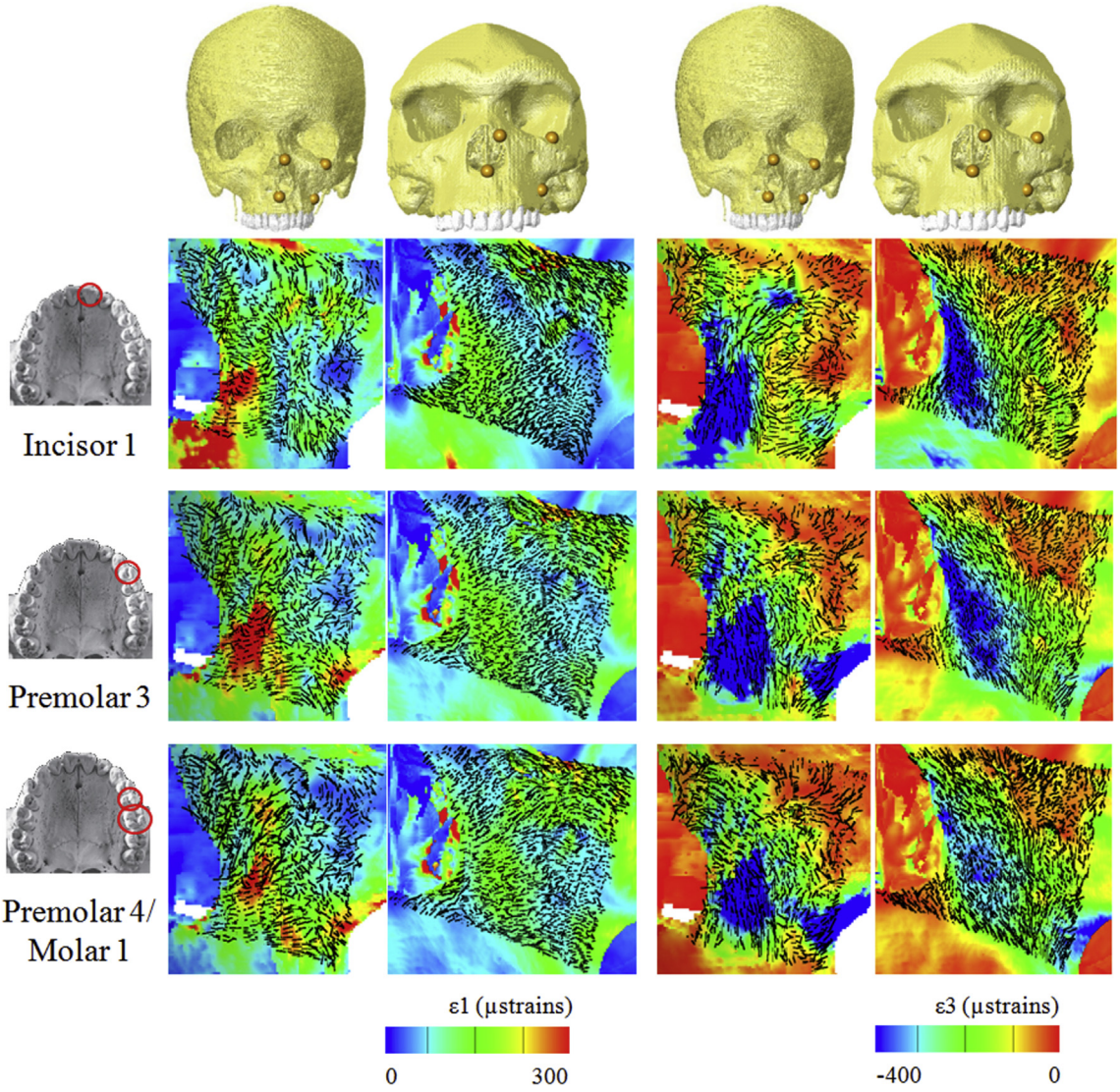

Figure 5. Principal strain magnitudes and directions of ε1 and ε3 in *Homo sapiens* and Broken Hill under different simulated bites (over the area delimited by the four landmarks shown on the crania in row 1). Column 1 identifies each of the simulated bites (last row depicts fourth premolar bite for Broken Hill and first molar for *H. sapiens*). The results for *H. sapiens* are presented in column 2 (ε1) and 4 (ε3). The results for Broken Hill are presented in column 3 (ε1) and 5 (ε3).

distributions of regions of high and low strain were found to be generally consistent across all specimens for both their third premolar and second molar biting simulations (Ledogar et al., 2016a:Figs. 7 and 8). Further, the strain contour maps they obtained (Ledogar et al., 2016a:Fig. 7) for the third premolar bite closely mirror those found here for the same bite. Maximum principal strains of approximately 280 με and minimum of ~ −600 με were found among their models. These values are comparable to, but not the same as found in our modern human. However, as noted earlier, great care must be taken when comparing predicted strain magnitudes among models built using different protocols, and protocols certainly differ between the present study and that of Ledogar et al. (2016a). In particular, their models are built with a wide range of material properties, whereas ours are simplified to consist of a single homogenous isotropic material, based on the prior validation and sensitivity work of Toro-Ibacache et al. (2016a) and Godinho et al. (2017).

Likewise, Toro-Ibacache et al. (2016b) performed FEAs using the same protocol as in the present study on two crania representing the extremes of shape variation in a sample of 20 adult modern humans. For identical bite forces of 350 N at the central incisors, and 700 N at M^1, Toro-Ibacache et al. (2016b) also found a similar distribution of strains between the two individuals, comparable with other studies in human and non-human primates. Peak strains for these same individuals loaded with their own muscle forces (i.e., not necessarily generating identical bite forces) ranged from ~400 με (ε1) and −450 (ε3) for I^1 bites, and ~350 με (ε1) and −300 (ε3) for M^1 bites.

The strain magnitudes and strain contour maps from premolar bites presented in Ledogar et al. (2016a) and Toro-Ibacache et al. (2016b) are comparable with those developed in our single modern human model, with maximum principal strain (ε1) of 468 με and minimum (ε3) of −302 με. In comparison, Broken Hill loaded with the same muscle forces as our modern human achieves in premolar bite a maximum principal strain (ε1) of 241 με and minimum (ε3) of −144 με. These figures are approximately 50% and 48% respectively of those achieved in our modern human model built using identical protocols. This supports our conclusion that the strains developed in Broken Hill are substantially less than those found in modern humans during simulated biting.

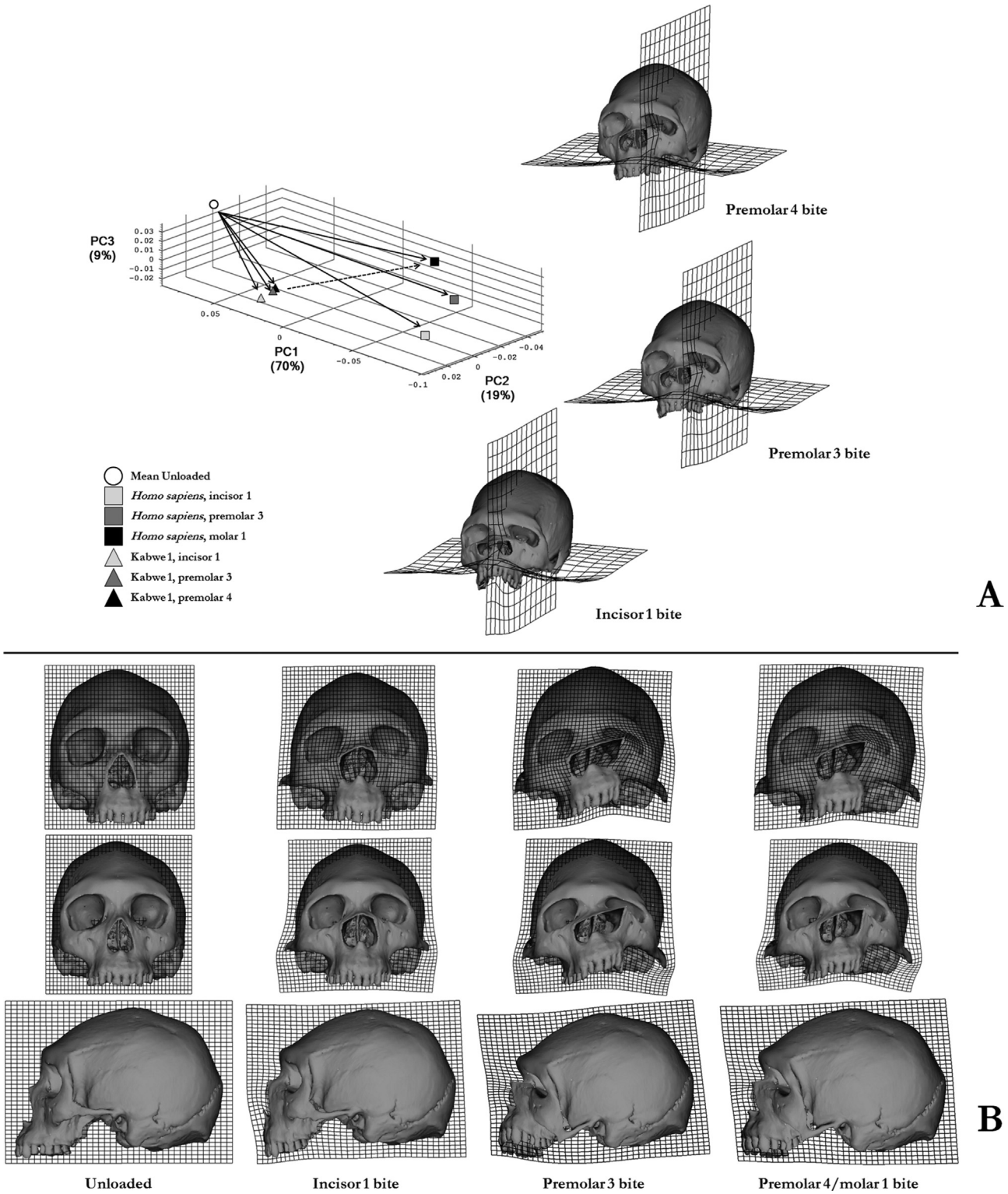

Figure 6. Size and shape analysis of modes and magnitudes of deformation of the models with the magnitudes of deformation of Broken Hill scaled according to the ratio of bite forces and the inverse of the ratio of facial centroid sizes. Reference cranium used for warpings is the mean unloaded cranium calculated from the unloaded crania of Broken Hill and *Homo sapiens*. A) Size and shape PCA plot with warpings of different load cases of *H. sapiens* relative to the mean unloaded model, B) Surface warpings with transformation grids located at the nasal cavity (first row), zygomatic arches (second row) and midline (third row), illustrating the differences in deformation due to biting between loaded Broken Hill (reference) and loaded *H. sapiens* (target; see dotted arrow representing the difference in molar bites). These deformations and so the grids and warped surfaces are exaggerated by a factor of $\times$ 500.

Identical modelling and loading protocols to those used in this study were also used in a related study (Toro-Ibacache, 2014). Twenty crania were reconstructed from clinical CTs of living Chileans. FE models of four individuals representing the extremes of variation, including sex differences, as assessed by PCA, were built and loaded. The resulting strain maps vary in ways that are very similar to those found by Ledogar et al. (2016a) indicating similar modes and magnitudes of deformation. Further, the modern human cranium used in the present study is unremarkable in terms of strain magnitudes and the distribution of regions of high and low strains. This gives us confidence that our modern human model behaves in an unexceptional way when compared to other modern humans. In contrast, the Broken Hill cranium develops peak strains that are approximately half of the magnitude of those developed in modern humans and the average strains at all sampled loci are approximately 1/3 of those found in the modern human. In consequence, we are confident that the differences we estimate in overall strain magnitudes between the specimen of *H. sapiens* and Broken Hill reflect a real difference between groups, as opposed to interindividual variation within a group.

4.3. Is increased biting efficiency in modern humans the result of adaptation?

The present findings are consistent with previous studies that have compared *H. sapiens* with *H. heidelbergensis* and Neanderthals, in that modern humans appear more efficient at converting muscle forces into bite forces due to a retracted and orthognathic face (Antón, 1990; O'Connor et al., 2005; Lieberman, 2008, 2011; Eng et al., 2013). Antón (1990) and Eng et al. (2013) found that *H. sapiens* is able to produce higher absolute bite forces than Neanderthals, while O'Connor et al. (2005) estimated that Neanderthals generate higher absolute bite forces than recent gracile modern humans and comparable to early and recent robust *H. sapiens* because of increased muscle forces. Facial reduction in *H. sapiens*, which increases mechanical efficiency in bite force generation, has been suggested to be accompanied by the cranium of *H. sapiens* being generally less able to resist masticatory, or paramasticatory, functional loading (Rak, 1986; Demes, 1987; Lieberman, 2008, 2011; Ledogar et al., 2016a). This, together with a decrease in the proportion of fast twitch muscle fibres (Stedman et al., 2004) relative to apes and size reduction of masticatory muscles (Demes and Creel, 1988; Antón, 1990; O'Connor et al., 2005) led Lieberman (2008, 2011) to propose that selection of these anatomical features is likely unrelated to mastication and increased mechanical advantage in *H. sapiens*.

The human cranium shows a degree of integration (Bastir and Rosas, 2005; Lieberman, 2008, 2011; Neaux et al., 2013, 2015; Bastir and Rosas, 2016), which implies that evolutionary and adaptive changes in one component of the cranium impact other components (Lieberman, 2008, 2011). As such, changes in facial morphology throughout hominin evolution have been suggested to be related to multiple factors, including expansion of the brain and an increased cranial base angle (Enlow and Hans, 1996; Lieberman et al., 2002; Lieberman, 2008, 2011), thermoregulation and air conditioning (Coon, 1962; Wolpoff, 1968; Carey and Steegmann, 1981; Franciscus and Trinkaus, 1988), preprocessing of food (Carlson, 1976; Carlson and Van Gerven, 1977), stabilization of the head during running (Lieberman, 2008, 2011) and reduction in size of the dentition (Brace, 1967; Brace and Mahler, 1971; Brace et al., 1987). Distinguishing the possibilities that evolutionary origin of facial reduction, retraction and orthognathy is the outcome of positive selection and adaptation from the alternative that they are an evolutionary by-product (Gould and Lewontin, 1979; Lieberman, 2008, 2011) is therefore extremely difficult. In fact, relative to increased bite force efficiency and capability the facial reduction of *H. sapiens* may be an exaptation (sensu Gould and Vrba, 1982), i.e., a feature co-opted during evolution to perform such function (thereby increasing fitness), irrespective of whether it was originally selected to perform another function or whether it evolved as a non-adaptive byproduct. Preprocessing of food items (see below) may have precluded the need to generate and/or use such high bite forces and so, the notion that this ability might have been selectively advantageous (thereby discounting it as a result of either adaptation or exaptation).

In addition, genetic drift has been suggested to impact on the overall cranial morphology of early *Homo* (Ackermann and Cheverud, 2004) and in modern humans (Weaver et al., 2007; Weaver and Stringer, 2015), albeit less so in specific anatomical regions such as the nose (Roseman and Weaver, 2004), which fulfils functions related to metabolic aerobic demands (Lindsay, 1996; Bastir and Rosas, 2013), olfaction (Lindsay, 1996; Bastir and Rosas, 2013), thermoregulation (Trinkaus, 1987b; Dean, 1988; Franciscus and Trinkaus, 1988) and conditioning of respired air (Franciscus and Long, 1991; Yokley, 2009; Lieberman, 2011; Noback et al., 2011). Reduction of the size of the nasal cavity in *H. sapiens* inevitably impacts midfacial morphology and therefore biting performance. This reduction may have arisen through neutral evolutionary processes or selection, although it is not clear what the selective pressure(s) might have been. Alternatively, a large midface and tall, deep nasal cavity may have been positively selected for in archaic *Homo*, with a large nasal cavity being required either for air conditioning or to accommodate the metabolic demands of a possibly larger body in other extinct species of *Homo* (Yokley et al., 2009; Lieberman, 2011; Churchill, 2014; but see, for limitations of body mass estimation from skeletal elements, Elliot et al., 2014; Heyes and MacDonald, 2015) and therefore might have constrained the form, and so, functioning of the masticatory system. Thus, a larger midface leads to mechanical advantages of the masticatory muscles in *H. heidelbergensis* that are less than those in subsequent *H. sapiens,* where this constraint is released. If the morphology of the nose was indeed constrained in *H. heidelbergensis* and the constraint was released in *H. sapiens*, enabling midfacial retraction, then the increased biting precision and force production efficiency of modern humans would be an incidental consequence of changes in midfacial morphology.

An alternative evolutionary scenario for midfacial reduction has been proposed, in which culturally acquired food processing technologies would have reduced selective pressure on the jaws to resist large and/or repetitive masticatory loading (e.g., Zink and Lieberman, 2016). From this perspective, it could be argued that the preprocessing of food to soften or break it up also releases constraints on the need for wide gapes and so larger jaws, advantageous in the oral acquisition of large food items (see also Zink and Lieberman, 2016, with regard to the impact of slicing food items for chewing efficiency in early *Homo*). However, further research is needed to investigate the potential trade-off between facial reduction (i.e., anteroposterior length of the nasal cavity and maxilla), gape and biting force, and their interaction with food preparation technologies among archaic and modern humans.

Whichever hypothesis is correct, the jaws of modern humans show a mismatch between increased mechanical advantage and potential maximum bite forces, on the one hand, and no consistently increased ability to resist forces, on the other, even considering differences in facial size and muscle force. This is because the jaws are rarely, if ever, tasked with generating and resisting

maximal bite forces and, indeed, older modern and fossil *Homo* edentulous individuals demonstrate that the survival of humans is less dependent on masticatory system mechanical functioning than on food preparation.

It is worth noting two potential consequences of facial reduction in *H. sapiens*. The first is a direct outcome of *H. sapiens* possessing shorter out-relative to in-levers when compared to *H. heidelbergensis*. The mechanical advantages (Table 3) of masticatory muscles in incisor bites differ by 10–50% with an average of 32.5%, indicating that precision of mechanical control of incisors is approximately 30–35% greater in the modern human model. The significance of this with regard to feeding and use of the anterior dentition as tools is unknown but, is an interesting question for future studies. The second possible anatomical consequence of midfacial reduction in *H. sapiens* is the development of the chin. Its presence has been associated with multiple factors (Horowitz and Thompson, 1964; Wolff, 1984; Ichim et al., 2007; Thayer and Dobson, 2010; Pampush, 2015) and with mechanical demands during biting and mastication (Daegling, 1993; Dobson and Trinkaus, 2002; Groning et al., 2011). However, recent studies question the extent to which the modern human symphysis and chin are optimized to resist masticatory system loads and suggest that, rather than being adaptive, it may be a by-product (Holton et al., 2014, 2015; Pampush and Daegling, 2016) of midfacial reduction. In this scenario, midfacial reduction results in posterior retraction of the alveolus relative to the basal part of the mandible due to occlusal interlocking and this is accommodated by resorptive activity in the alveolar region with depositional activity in the basal (Enlow and Hans, 1996), a pattern of remodelling that may well covary with the presence of a chin among recent hominins (Lacruz et al., 2013, 2015).

Regardless of the causes of midfacial retraction in *H. sapiens*, it is clear that the masticatory system of modern humans converts muscle into bite forces more efficiently, yet is not better able to resist these forces than in the hypothesized ancestral species, *H. heidelbergensis*.

5. Conclusions

Our results are consistent with previous studies showing that *H. sapiens* is more efficient in converting muscle force into bite force than its hypothesized ancestral species, *H. heidelbergensis*. This results in greater predicted bite forces in the modern human than in Broken Hill. Conversely, the *H. sapiens* model shows decreased ability to resist masticatory loading when size and muscle force differences are accounted for, thus suggesting that increased masticatory efficiency is an incidental result of facial reduction, which may be driven by other factors, and plausibly had other consequences such as the formation of a chin. What these factors are and if they themselves are the result of adaptation rather than neutral evolutionary processes requires further study.

Acknowledgements

Ricardo Miguel Godinho was funded by the Portuguese Foundation for Science and Technology (FCT; PhD funding reference: SFRH/BD/76375/2011). Chris Stringer's research is supported by the Calleva Foundation and the Human Origins Research Fund of the Natural History Museum. We thank Robert Kruszynski, Natural History Museum, London, UK, for access to the CT scan of Broken Hill I and to the original fossil. We thank Professor Gerhard Weber, Department of Anthropology, University of Vienna, Austria and Professor George D. Koufos, Department of Geology, Aristotle University of Thessaloniki, Greece for access to the CT scan of Petralona. We are grateful to Dr. William Sellers, University of Manchester, UK, for providing us with access to software in his laboratory to facilitate mesh reconstruction of fossils and to Professor Chris Klingenberg also of the University of Manchester for vigorous discussions that improved the SOM of this paper.

Supplementary Online Material

Supplementary online material related to this article can be found at https://doi.org/10.1016/j.jhevol.2018.02.010.

References

Ackermann, R.R., Cheverud, J.M., 2004. Detecting genetic drift versus selection in human evolution. Proceedings of the National Academy of Sciences USA 101, 17946–17951.
Antón, S.C., 1990. Neandertals and the anterior dental loading hypothesis: a biomechanical evaluation of bite force production. Kroeber Anthropological Society Papers 71–72, 67–76.
Antón, S.C., 1996. Tendon-associated bone features of the masticatory system in Neandertals. Journal of Human Evolution 31, 391–408.
Baab, K.L., McNulty, K.P., 2009. Size, shape, and asymmetry in fossil hominins: The status of the LB1 cranium based on 3D morphometric analyses. Journal of Human Evolution 57, 608–622.
Bastir, M., Rosas, A., 2005. Hierarchical nature of morphological integration and modularity in the human posterior face. American Journal of Physical Anthropology 128, 26–34.
Bastir, M., Rosas, A., 2013. Cranial airways and the integration between the inner and outer facial skeleton in humans. American Journal of Physical Anthropology 152, 287–293.
Bastir, M., Rosas, A., 2016. Cranial base topology and basic trends in the facial evolution of *Homo*. Journal of Human Evolution 91, 26–35.
Bird, J., Ross, C., 2012. Mechanical Engineering Principles. Routledge, New York.
Brace, C.L., 1967. Environment, tooth form, and size in the Pleistocene. Journal of Dental Research 46, 809–816.
Brace, C.L., Mahler, P.E., 1971. Post-Pleistocene changes in the human dentition. American Journal of Physical Anthropology 34, 191–203.
Brace, C.L., Rosenberg, K.R., Hunt, K.D., 1987. Gradual change in human tooth size in the late Pleistocene and post-Pleistocene. Evolution 41, 705–720.
Bräuer, G., 2001. The 'Out-of-Africa' model and the question of regional continuity. In: Tobias, P.V. (Ed.), Humanity from African Naissance to Coming Millennia. Firenze University Press, Firenze, pp. 183–189.
Bright, J.A., Rayfield, E.J., 2011. Sensitivity and ex vivo validation of finite element models of the domestic pig cranium. Journal of Anatomy 219, 456–471.
Carey, J.W., Steegmann, A.T., 1981. Human nasal protrusion, latitude, and climate. American Journal of Physical Anthropology 56, 313–319.
Carlson, D.S., 1976. Temporal variation in prehistoric Nubian crania. American Journal of Physical Anthropology 45, 467–484.
Carlson, D.S., Van Gerven, D.P., 1977. Masticatory function and post-Pleistocene evolution in Nubia. American Journal of Physical Anthropology 46, 495–506.
Churchill, S.E., 2014. Thin on the Ground: Neandertal Biology. Archeology and Ecology. Wiley-Blackwell, Hoboken.
Clement, A.F., Hillson, S.W., Aiello, L.C., 2012. Tooth wear, Neanderthal facial morphology and the anterior dental loading hypothesis. Journal of Human Evolution 62, 367–376.
Coon, C.S., 1962. The Origin of Races. Knopf, New York.
Daegling, D.J., 1993. Functional morphology of the human chin. Evolutionary Anthropology 1, 170–177.
Dean, M.C., 1988. Another look at the nose and the functional significance of the face and nasal mucous membrane for cooling the brain in fossil hominids. Journal of Human Evolution 17, 715–718.
Dechow, P.C., Nail, G.A., Schwartz-Dabney, C.L., Ashman, R.B., 1993. Elastic properties of human supraorbital and mandibular bone. American Journal of Physical Anthropology 90, 291–306.
Demes, B., 1987. Another look at an old face: biomechanics of the neandertal facial skeleton reconsidered. Journal of Human Evolution 16, 297–303.
Demes, B., Creel, N., 1988. Bite force, diet, and cranial morphology of fossil hominids. Journal of Human Evolution 17, 657–670.
Dobson, S.D., Trinkaus, E., 2002. Cross-sectional geometry and morphology of the mandibular symphysis in Middle and Late Pleistocene *Homo*. Journal of Human Evolution 43, 67–87.
Dumont, E.R., Grosse, I.R., Slater, G.J., 2009. Requirements for comparing the performance of finite element models of biological structures. Journal of Theoretical Biology 256, 96–103.
Elliott, M., Kurki, H., Weston, D.A., Collard, M., 2014. Estimating fossil hominin body mass from cranial variables: an assessment using CT data from modern humans of known body mass. American Journal of Physical Anthropology 154, 201–214.
Enlow, D.H., Hans, M.G., 1996. Essentials of Facial Growth. W. B. Saunders Company, Philadelphia.
Enlow, D.H., McNamara, J.A., 1973. The neurocranial basis for facial form and pattern. The Angle Orthodontist 43, 256–270.

Eng, C.M., Lieberman, D.E., Zink, K.D., Peters, M.A., 2013. Bite force and occlusal stress production in hominin evolution. American Journal of Physical Anthropology 151, 544–557.
Fagan, M.J., Curtis, N., Dobson, C.A., Karunanayake, J.H., Kupczik, K., Moazen, M., Page, L., Phillips, R., O'Higgins, P., 2007. Voxel-based finite element analysis – Working directly with microCT scan data. Journal of Morphology 268, 1071–1071.
Fitton, L.C., Shi, J.F., Fagan, M.J., O'Higgins, P., 2012. Masticatory loadings and cranial deformation in *Macaca fascicularis*: A finite element analysis sensitivity study. Journal of Anatomy 221, 55–68.
Fitton, L.C., Prôa, M., Rowland, C., Toro-Ibacache, V., O'Higgins, P., 2015. The impact of simplifications on the performance of a finite element model of a *Macaca fascicularis* cranium. The Anatomical Record 298, 107–121.
Franciscus, R.G., Long, J.C., 1991. Variation in human nasal height and breadth. American Journal of Physical Anthropology 85, 419–427.
Franciscus, R.G., Trinkaus, E., 1988. The Neandertal nose. American Journal of Physical Anthropology 75, 209–210.
Freidline, S.E., Gunz, P., Harvati, K., Hublin, J.J., 2012. Middle Pleistocene human facial morphology in an evolutionary and developmental context. Journal of Human Evolution 63, 723–740.
Godinho, R.M., O'Higgins, P., 2017. Virtual reconstruction of cranial remains: The *H. heidelbergensis*, Kabwe 1 fossil. In: Thompson, T., Errickson, D. (Eds.), Human Remains: Another Dimension. The Application of Imaging to the Study of Human Remains. Academic Press, London, pp. 135–147.
Godinho, R.M., Toro-Ibacache, V., Fitton, L.C., O'Higgins, P., 2017. Finite element analysis of the cranium: Validity, sensitivity and future directions. Comptes Rendus Palevol 16, 600–612.
Gould, S.J., Lewontin, R.C., 1979. The spandrels of San Marco and the panglossian paradigm: a critique of the adaptationist programme. Proceedings of the Royal Society of London B 205, 581–598.
Gould, S.J., Vrba, E.S., 1982. Exaptation—A missing term in the science of form. Paleobiology 8, 4–15.
Groning, F., Liu, J., Fagan, M.J., O'Higgins, P., 2011. Why do humans have chins? Testing the mechanical significance of modern human symphyseal morphology with finite element analysis. American Journal of Physical Anthropology 144, 593–606.
Grosse, I.R., Dumont, E.R., Coletta, C., Tolleson, A., 2007. Techniques for modeling muscle-induced forces in finite element models of skeletal structures. The Anatomical Record 290, 1069–1088.
Heyes, P., MacDonald, K., 2015. Neandertal energetics: uncertainty in body mass estimation limits comparisons with *Homo sapiens*. Journal of Human Evolution 85, 193–197.
Holton, N.E., Franciscus, R.G., Ravosa, M.J., Southard, T.E., 2014. Functional and morphological correlates of mandibular symphyseal form in a living human sample. American Journal of Physical Anthropology 153, 387–396.
Holton, N.E., Bonner, L.L., Scott, J.E., Marshall, S.D., Franciscus, R.G., Southard, T.E., 2015. The ontogeny of the chin: an analysis of allometric and biomechanical scaling. Journal of Anatomy 226, 549–559.
Horowitz, S.L., Thompson Jr., R.H., 1964. Variations of the craniofacial skeleton in postadolescent males and females. The Angle Orthodontist 34, 97–102.
Hublin, J.-J., Ben-Ncer, A., Bailey, S.E., Freidline, S.E., Neubauer, S., Skinner, M.M., Bergmann, I., Le Cabec, A., Benazzi, S., Harvati, K., Gunz, P., 2017. New fossils from Jebel Irhoud, Morocco and the pan-African origin of *Homo sapiens*. Nature 546, 289–292.
Ichim, P., Kieser, J., Swain, M., 2007. Tongue contractions during speech may have led to the development of the bony geometry of the chin following the evolution of human language: a mechanobiological hypothesis for the development of the human chin. Medical Hypotheses 69, 20–24.
La Cruz, R.S., Bermúdez de Castro, J.M., Martinón-Torres, M., O'Higgins, P., Paine, M.L., Carbonell, E., Arsuaga, J.L., Bromage, T.G., 2013. Facial morphogenesis of the earliest Europeans. PLoS One 8, e65199.
Lacruz, R.S., Bromage, T.G., O'Higgins, P., Arsuaga, J.-L., Stringer, C., Godinho, R.M., Warshaw, J., Martínez, I., Gracia-Tellez, A., Bermúdez de Castro, J.M., Carbonell, E., 2015. Ontogeny of the maxilla in Neanderthals and their ancestors. Nature Communications 6, 8996.
Laird, M.F., Vogel, E.R., Pontzer, H., 2016. Chewing efficiency and occlusal functional morphology in modern humans. Journal of Human Evolution 93, 1–11.
Ledogar, J.A., Dechow, P.C., Wang, Q., Gharpure, P.H., Gordon, A.D., Baab, K.L., Smith, A.L., Weber, G.W., Grosse, I.R., Ross, C.F., Richmond, B.G., 2016a. Human feeding biomechanics: performance, variation, and functional constraints. PeerJ 4 e2242.
Ledogar, J.A., Smith, A.L., Benazzi, S., Weber, G.W., Spencer, M.A., Carlson, K.B., McNulty, K.P., Dechow, P.C., Grosse, I.R., Ross, C.F., Richmond, B.G., 2016b. Mechanical evidence that *Australopithecus sediba* was limited in its ability to eat hard foods. Nature Communications 7, 10596.
Ledogar, J.A., Benazzi, S., Smith, A.L., Weber, G.W., Carlson, K.B., Dechow, P.C., Grosse, I.R., Ross, C.F., Richmond, B.G., Wright, B.W., Wang, Q., Byron, C., Carlson, K.J., De Ruiter, D.J., Pryor Mcintosh, L.C., Strait, D.S., 2017. The biomechanics of bony facial "buttresses" in South African australopiths: An experimental study using finite element analysis. The Anatomical Record 300, 171–195.
Lieberman, D., 2011. The Evolution of the Human Head. Harvard University Press, Cambridge.
Lieberman, D.E., 2008. Speculations about the selective basis for modern human craniofacial form. Evolutionary Anthropology 17, 55–68.
Lieberman, D.E., McBratney, B.M., Krovitz, G., 2002. The evolution and development of cranial form in *Homo sapiens*. Proceedings of the National Academy of Sciences USA 99, 1134–1139.
Lindsay, D.T., 1996. Functional Human Anatomy. Mosby-Year Book, St. Louis.
Meyer, M., Arsuaga, J.-L., de Filippo, C., Nagel, S., Aximu-Petri, A., Nickel, B., Martínez, I., Gracia, A., Bermúdez de Castro, J.M., Carbonell, E., Viola, B., Kelso, J., Prüfer, K., Pääbo, S., 2016. Nuclear DNA sequences from the Middle Pleistocene Sima de los Huesos hominins. Nature 531, 504–507.
Milne, N., O'Higgins, P., 2012. Scaling of form and function in the xenarthran femur: A 100-fold increase in body mass is mitigated by repositioning of the third trochanter. Proceedings of the Royal Society B 279, 3449–3456.
Neaux, D., Guy, F., Gilissen, E., Coudyzer, W., Ducrocq, S., 2013. Covariation between midline cranial base, lateral basicranium, and face in modern humans and chimpanzees: A 3D geometric morphometric analysis. The Anatomical Record 296, 568–579.
Neaux, D., Gilissen, E., Coudyzer, W., Guy, F., 2015. Integration between the face and the mandible of *Pongo* and the evolution of the craniofacial morphology of orangutans. American Journal of Physical Anthropology 158, 475–486.
Noback, M.L., Harvati, K., Spoor, F., 2011. Climate-related variation of the human nasal cavity. American Journal of Physical Anthropology 145, 599–614.
O'Connor, C.F., Franciscus, R.G., Holton, N.E., 2005. Bite force production capability and efficiency in neandertals and modern humans. American Journal of Physical Anthropology 127, 129–151.
O'Higgins, P., Cobb, S.N., Fitton, L.C., Groning, F., Phillips, R., Liu, J., Fagan, M.J., 2011. Combining geometric morphometrics and functional simulation: an emerging toolkit for virtual functional analyses. Journal of Anatomy 218, 3–15.
O'Higgins, P., Fitton, L.C., Phillips, R., Shi, J.F., Liu, J., Groning, F., Cobb, S.N., Fagan, M.J., 2012. Virtual functional morphology: novel approaches to the study of craniofacial form and function. Evolutionary Biology 39, 521–535.
O'Higgins, P., Milne, N., 2013. Applying geometric morphometrics to compare changes in size and shape arising from finite elements analyses. Hystrix 24, 126–132.
Pampush, J.D., 2015. Selection played a role in the evolution of the human chin. Journal of Human Evolution 82, 127–136.
Pampush, J.D., Daegling, D.J., 2016. The enduring puzzle of the human chin. Evolutionary Anthropology 25, 20–35.
Rak, Y., 1986. The Neanderthal: A new look at an old face. Journal of Human Evolution 15, 151–164.
Rightmire, G.P., 1998. Human evolution in the middle Pleistocene: The role of *Homo heidelbergensis*. Evolutionary Anthropology 6, 218–227.
Rightmire, G.P., 2013. *Homo erectus* and Middle Pleistocene hominins: Brain size, skull form, and species recognition. Journal of Human Evolution 65, 223–252.
Roseman, C.C., Weaver, T.D., 2004. Multivariate apportionment of global human craniometric diversity. American Journal of Physical Anthropology 125, 257–263.
Ross, C.F., Patel, B.A., Slice, D.E., Strait, D.S., Dechow, P.C., Richmond, B.G., Spencer, M.A., 2005. Modeling masticatory muscle force in finite element analysis: Sensitivity analysis using principal coordinates analysis. The Anatomical Record 283A, 288–299.
Schwartz-Dabney, C.L., Dechow, P.C., 2003. Variations in cortical material properties throughout the human dentate mandible. American Journal of Physical Anthropology 120, 252–277.
Schwartz, J.H., Tattersall, I., 2003. Craniodental Morphology of Genus *Homo* (Africa and Asia). The Human Fossil Record, vol. 2. Wiley-Liss, Hoboken.
Smith, A.L., Benazzi, S., Ledogar, J.A., Tamvada, K., Pryor Smith, L.C., Weber, G.W., Spencer, M.A., Lucas, P.W., Michael, S., Shekeban, A., Al-Fadhalah, K., 2015. The feeding biomechanics and dietary ecology of *Paranthropus boisei*. The Anatomical Record 298, 145–167.
Spencer, M.A., Demes, B., 1993. Biomechanical analysis of masticatory system configuration in Neandertals and Inuits. American Journal of Physical Anthropology 91, 1–20.
Stedman, H.H., Kozyak, B.W., Nelson, A., Thesier, D.M., Su, L.T., Low, D.W., Bridges, C.R., Shrager, J.B., Minugh-Purvis, N., Mitchell, M.A., 2004. Myosin gene mutation correlates with anatomical changes in the human lineage. Nature 428, 415–418.
Strait, D.S., Grosse, I.R., Dechow, P.C., Smith, A.L., Wang, Q., Weber, G.W., Neubauer, S., Slice, D.E., Chalk, J., Richmond, B.G., Lucas, P.W., Spencer, M.A., Schrein, C., Wright, B.W., Byfton, C., Ross, C.F., 2010. The structural rigidity of the cranium of *Australopithecus africanus*: implications for diet, dietary adaptations, and the allometry of feeding biomechanics. The Anatomical Record 293, 583–593.
Strait, D.S., Richmond, B.G., Spencer, M.A., Ross, C.F., Dechow, P.C., Wood, B.A., 2007. Masticatory biomechanics and its relevance to early hominid phylogeny: an examination of palatal thickness using finite-element analysis. Journal of Human Evolution 52, 585–599.
Strait, D.S., Weber, G.W., Neubauer, S., Chalk, J., Richmond, B.G., Lucas, P.W., Spencer, M.A., Schrein, C., Dechow, P.C., Ross, C.F., Grosse, I.R., Wright, B.W., Constantino, P., Wood, B.A., Lawn, B., Hylander, W.L., Wang, Q., Byron, C., Slice, D.E., Smith, A.L., 2009. The feeding biomechanics and dietary ecology of *Australopithecus africanus*. Proceedings of the National Academy of Sciences USA 106, 2124–2129.
Stringer, C.B., 1983. Some further notes on the morphology and dating of the Petralona hominid. Journal of Human Evolution 12, 731–742.
Stringer, C., 2012. The status of *Homo heidelbergensis* (Schoetensack 1908). Evolutionary Anthropology 21, 101–107.
Stringer, C., 2016. The origin and evolution of *Homo sapiens*. Philosophical Transactions of the Royal Society B 371, 20150237.

Tappen, N.C., 1978. The vermiculate surface pattern of brow ridges in Neandertal and modern crania. American Journal of Physical Anthropology 49, 1–10.
Thayer, Z.M., Dobson, S.D., 2010. Sexual dimorphism in chin shape: implications for adaptive hypotheses. American Journal of Physical Anthropology 14, 417–425.
Toro-Ibacache, V., 2014. A finite element study of the human cranium; the impact of morphological variation on biting performance. Ph.D. Dissertation, Hull York Medical School and University of York.
Toro-Ibacache, V., Zapata Muñoz, V., O'Higgins, P., 2015. The predictability from skull morphology of temporalis and masseter muscle cross-sectional areas in humans. The Anatomical Record 298, 1261–1270.
Toro-Ibacache, V., Fitton, L.C., Fagan, M.J., O'Higgins, P., 2016a. Validity and sensitivity of a human cranial finite element model: implications for comparative studies of biting performance. Journal of Anatomy 228, 70–84.
Toro-Ibacache, V., O'Higgins, P., 2016. The effect of varying jaw-elevator muscle forces on a finite element model of a human cranium. The Anatomical Record 299, 828–839.
Toro-Ibacache, V., Zapata Muñoz, V., O'Higgins, P., 2016b. The relationship between skull morphology, masticatory muscle force and cranial skeletal deformation during biting. Annals of Anatomy 203, 59–68.
Trinkaus, E., 1987a. The Neandertal face: evolutionary and functional perspectives on a recent hominid face. Journal of Human Evolution 16, 429–443.
Trinkaus, E., 1987b. Bodies, brawn, brains and noses: human ancestors and human predation. In: Nitecki, M., Nitecki, D. (Eds.), The Evolution of Human Hunting. Springer, New York, pp. 107–145.
Trinkaus, E., 2003. Neandertal faces were not long; modern human faces are short. Proceedings of the National Academy of Sciences USA 100, 8142–8145.
Weaver, T.D., Stringer, C.B., 2015. Unconstrained cranial evolution in Neandertals and modern humans compared to common chimpanzees. Proceedings of the Royal Society B 282, 20151519.
Weaver, T.D., Roseman, C.C., Stringer, C.B., 2007. Were Neandertal and modern human cranial differences produced by natural selection or genetic drift? Journal of Human Evolution 53, 135–145.
Winterton, R., 2006. The Human Tissue Act 2004 (Ethical approval, exceptions from Licensing and supply of information about transplants) Regulations 2006. The Stationery Officer Limited. http://www.legislation.gov.uk/uksi/2006/1260/pdfs/uksi_20061260_en.pdf.
Witzel, U., 2011. Virtual synthesis of the skull in Neanderthals by FESS. In: Condemi, S., Weniger, G.-C. (Eds.), Continuity and Discontinuity in the Peopling of Europe. Springer, Dordrecht, pp. 203–211.
Wolff, J.A., 1984. A theoretical approach to solve the chin problem. In: Chivers, D., Wood, B., Bilsborough, A. (Eds.), Food Acquisition and Processing in Primates. Springer, Boston, pp. 391–405.
Wolpoff, M.H., 1968. Climatic influence on skeletal nasal aperture. American Journal of Physical Anthropology 29, 405–423.
Wroe, S., Ferrara, T.L., McHenry, C.R., Curnoe, D., Chamoli, U., 2010. The craniomandibular mechanics of being human. Proceedings of the Royal Society B 277, 3579–3586.
Yokley, T.R., 2009. Ecogeographic variation in human nasal passages. American Journal of Physical Anthropology 138, 11–22.
Yokley, T., Holton, N., Franciscus, R., Churchill, S., 2009. The role of body mass in the evolution of the modern human nasofacial skeleton. PaleoAnthropology A39–A40.
Zink, K.D., Lieberman, D.E., 2016. Impact of meat and Lower Palaeolithic food processing techniques on chewing in humans. Nature 531, 500–503.